Archaeological Prospection
Archaeol. Prospect. **11**, 1–18 (2004)
Published online 4 November 2003 in Wiley InterScience (www.interscience.wiley.com). DOI: 10.1002/arp.218

Two-dimensional Resistivity Imaging: a Tool in Archaeoseismology. An Example from Ancient Sagalassos (Southwest Turkey)†

DOMINIQUE SIMILOX-TOHON,[1,3]* KRIS VANNESTE,[2] MANUEL SINTUBIN,[1] PHILIPPE MUCHEZ[3] AND MARC WAELKENS[4]

[1] *Structural Geology and Tectonics Group, K.U. Leuven, Redingenstraat 16, 3000 Leuven, Belgium*
[2] *Royal Observatory of Belgium, Ringlaan 3, 1180 Brussel, Belgium*
[3] *Afdeling Fysico-chemische Geologie, K.U. Leuven, Celestijnenlaan 200C, 3001 Leuven, Belgium*
[4] *Department of Archaeology, K.U. Leuven, Blijde Inkomststraat 21, 3000 Leuven, Belgium*

ABSTRACT The ancient Pisidian town of Sagalassos (southwest Turkey) was struck by several earthquakes during Roman and early Byzantine times and was abandoned around the middle of the seventh century AD, partly as the result of a devastating earthquake. A nearby epicentre is postulated, although the causative fault has not yet been identified. The identification of such an active fault is, however, important with respect to the assessment of the seismic hazard of the area. Two-dimensional resistivity imaging has been used to detect the presence of an active normal fault passing underneath Sagalassos, as evidenced by geological, geomorphological and archaeoseismological observations. The resistivity profiles reveal the presence of five stratigraphical layers, i.e. from bottom to top: the bedrock composed of either limestone or ophiolitic mélange, the weathered top of this bedrock, old colluvial material, recent colluvial material that covers archaeological structures and recent scree deposits. The presence of active normal faults is, moreover, indicated by the displacement of the bedrock and the colluvial material on top of it. Offsets of archaeological structures at Sagalassos are likely to be the result of historical reactivations of these faults. The limestone front, overlooking Sagalassos from the north, probably corresponds to the degraded fault plane of the detected fault zone. Sagalassos was thus built on the hanging wall of an active normal fault. Two-dimensional resistivity imaging proved to be an efficient tool in archaeoseismology.

Key words: two-dimensional resistivity imaging; archaeoseismology; active normal fault; historical earthquakes; southwest Turkey

Introduction

Classic tools in archaeoseismology focus on buildings and damage data at archaeological sites to identify past seismic events (Stiros and Jones, 1996). However, a geological and/or palaeoseismological approach in search of ancient earthquakes often provides important information and is also needed (Galli and Galadini, 2001). This approach integrates damage data in a larger geodynamic framework, eventually enabling a seismic hazard assessment in a given region. The main purpose of such an approach is to identify the fault(s) responsible for the

* Correspondence to: D. Similox-Tohon, Structural Geology and Tectonics Group, K.U. Leuven, Redingenstraat 16, 3000 Leuven, Belgium.
E-mail: dominique.similox-tohon@geo.kuleuven.ac.be
† This paper was presented at the EIGG Conference, London, December 2002.

Received 7 March 2003
Accepted 10 July 2003

observed seismic event(s) on a site. The analysis of that particular active fault can subsequently teach us more about the time and magnitude of events not recorded in the archaeological history. (*Active faults* are those that have moved within the duration of the current tectonic regime. In the region around Sagalassos this regime started in Early Pliocene time (5 million years ago) (Bozkurt, 2001).) This approach results in the identification of the recurrence of major seismic events. Knowing the time of the last event, as well as the recurrency time of the major seismic events, eventually leads to an assessment of the seismic hazard of the region.

In this paper an example is given for the region of the town of Sagalassos, in ancient Pisidia, located some 10 km south-southwest of Isparta (southwest Turkey) (Figure 1). The town was prosperous from Hellenistic into late Roman times (Waelkens, 1993). It has been struck by several earthquakes during Roman and early Byzantine times and was abandoned around the middle of the seventh century AD, partly as the result of a devastating earthquake (Waelkens *et al.*, 2000). Based on the high intensity of this last event, as recorded in the archaeological relics, a nearby (<20 km) epicentre has been postulated (Sintubin *et al.*, 2003). The causative fault, however, has not been identified.

Geological, geomorphological and archaeoseismological evidence suggests that an active normal fault passes underneath ancient Sagalassos (Sintubin *et al.*, 2003). However, this evidence only represents surface data. A subsurface analysis was expected to provide concluding proof. We used two-dimensional resistivity imaging ('electric tomography') to check the presence of such a fault. This method yields a vertical section of the subsurface resistivity distribution. Because in some parts of the study area the bedrock consists of an ophiolitic mélange, other geophysical methods were excluded. Ground penetration radar (GPR) is probably not appropriate because large clasts within the ophiolitic

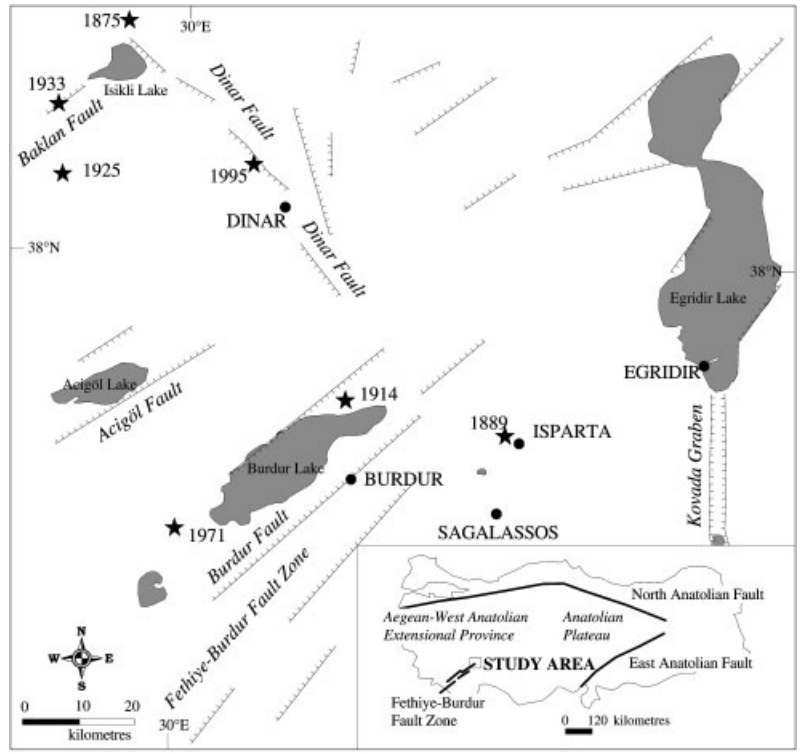

Figure 1. Neotectonic setting of ancient Sagalassos in southwest Turkey showing major structural elements (after Eyidogan and Barka, 1996; Bozkurt, 2001) and epicentres of recent major earthquakes (after Ambraseys and Jackson, 1998; Koral, 2000; Ambraseys, 2001; KOERI, 2002) (see Table 1).

mélange would cause too much disturbing diffraction. The topography is also too rough for continuous GPR profiling. Magnetic measurements probably would not work either, as the ophiolitic mélange, rich in magnetic minerals, would saturate the measurements. Moreover, the remote location of Sagalassos and the rough landscape forced us to use a relatively easy-to-handle method such as two-dimensional resistivity profiling.

Two-dimensional resistivity imaging has become increasingly popular over the past decade. The method, reasonably fast and cost-effective, is much more powerful than one-dimensional vertical electric sounding, which does not take into account horizontal changes in the subsurface resistivity. Electric tomography is now applied routinely for structural mapping, and also for hydrological and pollution surveys (Loke, 2001; Pellerin, 2002). Over the past few years, two-dimensional resistivity imaging has been applied in a number of palaeoseismological studies to locate and identify active faults. For instance in low-slip rate areas such as the Lower Rhine graben area (Western Europe), where the terrain is relatively flat and active faults have limited geomorphological expression, this approach has proven to be very successful (Demanet *et al*., 2001; Vanneste *et al*., 2002). At the site of Sagalassos, we expand our scope of application to a more mountainous terrain, where extensive slope processes and mass movements should be taken into consideration.

Electrical resistivity surveys have been used in archaeological investigations for many years (since the late 1950s) but generally have been restricted to the visualisation of resistivity values of the subsurface in a horizontal plane ('resistivity mapping') (Thacker *et al*., 2002). Only recently, has this method been used for determining the depth and geometry of archaeological bodies in a vertical section (Noel and Xu, 1991; Griffiths and Barker, 1994; Kampke, 1999; Sambuelli *et al*., 1999). In this paper the first result of two-dimensional resistivity measurements at Sagalassos are presented. With these results, we want to demonstrate the applicability of two-dimensional resistivity profiling in archaeoseismology.

Geological background

Sagalassos is located to the east of the seismically active Burdur graben system (Figure 1), characterized by three NE–SW trending half grabens, bounded by major northwest-dipping normal faults, the Burdur, Acıgöl and Baklan faults (Price and Scott, 1994). To the northeast, the graben system terminates against the NW–SE trending Dinar Fault, considered a break-away fault within this system. The Burdur graben system is located at the eastern edge of the extensional province of western Turkey and at the northeastern extremity of the Fethiye-Burdur Fault Zone (Barka *et al*., 1995).

Major earthquakes occurred in historical and recent times in this area but none of them resulted in any damage at Sagalassos (Table 1 and Figure 1). Historical records indicate earthquakes that affected the ancient city of Apamea Kibotos (the current Dinar) (Guidoboni *et al*., 1994).

Table 1. Major earthquakes around ancient Sagalassos (Guidoboni *et al.*, 1994; Eyidogan and Barka, 1996; Altunel *et al.*, 1999; Ambraseys and Jackson, 1998; Koral, 2000; Ambraseys, 2001; KOERI, 2002)

Date	Location	Fault	Ms	I_0
1500 BC	Apamea Kibotos (Dinar)	Dinar Fault	> 6.8	?
400 BC	Apamea Kibotos (Dinar)	?	?	?
88 BC	Apamea Kibotos (Dinar)	Dinar Fault	> 6.8	IX–XI
AD 53	Apamea Kibotos (Dinar)	?	?	VII–X
03.03.1875	Dinar	Baklan Fault	6.5	IX–X
17.01.1889	Isparta	?	Medium	Medium
03.10.1914	Burdur	Burdur Fault	7.0	IX
07.08.1925	Dinar	Baklan Fault	5.9	VII–IX
19.07.1933	Dinar	Baklan Fault	5.8	VIII
12.05.1971	Burdur	Burdur Fault	6.2	VIII
01.10.1995	Dinar	Dinar Fault	6.1	VIII

Recent earthquakes occurred on the Baklan, Dinar and Burdur Fault (Altunel *et al.*, 1999; Koral, 2000; Ambraseys, 2001). Fault plane solutions of the 1971 Burdur and 1995 Dinar earthquake indicate pure normal faulting (Taymaz and Price, 1992; Eyidogan and Barka, 1996). In 1889 a medium magnitude earthquake occurred near Isparta causing only local damage. The fault responsible, however, is not known (Ambraseys and Jackson, 1998).

Sagalassos is located on a south-facing undulating tectonized ophiolitic platform with limestone klippes and slumps on top (Degryse *et al.*, in press). Overlying allochtonous limestone nappes form the steep mountain ridge north of the town. This limestone front is characterized by extensive slope processes and mass movements (Librecht *et al.*, 2000; Verstraeten *et al.*, 2000). Scree material originating from this limestone front stretches out to the northern edge of the town. In the monumental part of Sagalassos, the ophiolitic mélange underlying the limestone klippes shows a subhorizontal geometry (Degryse *et al.*, in press).

Fault evidence at Sagalassos

To identify nearby active faults that could have been responsible for the ancient earthquakes at Sagalassos, satellite imagery and a digital elevation model were first analysed (Similox-Tohon *et al.*, 2002, 2003). The ENE–WSW trending limestone front, overlooking the town from the north, appears as a distinct linear feature. This lineament bears all the geomorphological features within resistant lithologies, as described in Goldsworthy and Jackson (2000), to be interpreted as an active normal fault (Similox-Tohon *et al.*, 2002, 2003), whereas it was previously interpreted as an older (pre-Quaternary) strike-slip fault (Poisson, 1977; Yalcinkaya, 1983). At the northwestern outskirts of the town, a necropolis has been carved in the mountain face that may correspond to a degraded fault plane (Figure 2) (Sintubin *et al.*, 2003).

Parallel to the mountain face, a lineament can be traced across the town based on a number of features (Figure 3) (Sintubin *et al.*, 2003).

Figure 2. Necropolis (indicated by ellipses) at the northwestern outskirts of Sagalassos. The mountain face may correspond to a degraded fault plane (cf. Sintubin *et al.*, 2003).

(i) A fault crack, filled with clay gouge, is present in the limestone bedrock of the Doric Temple (Figure 4). This fault has a N68°E trend and dips 65° towards the south. Tension gashes are present, indicative for normal faulting. It is not clear if the fault can be traced in the pavement of the Bouleuterion.

(ii) In a trench at the northeastern extremity of the Upper Agora a small normal fault has been observed in the tuffaceous bedrock (Paulissen E., Geomorphology and Regional Geography Group, K. U. Leuven, Belgium, personal communication, 2000).

(iii) Evidence of normal faulting is present in both the mosaic floor and the walls of the Neon Library (Waelkens *et al.*, 2000), where a bundle of N87°E trending cracks is observed, which throw the southern part of the floor a few centimetres downward (Figure 5).

(iv) A topographic scarp (ca. 2 m high, N80°E and south dipping) is observed at the eastern side of the town (Figure 6). Similar scarps have been detected on the digital elevation model of the town.

The alignment of all these features suggests that an active normal fault trace crosses ancient Sagalassos. One kilometre further east, a displaced (ca. 7 m) aqueduct clearly indicates normal fault activity in historical times (Steegen *et al.*, 2000; Verstraeten *et al.*, 2000). Two parallel aqueducts are present at different heights in the displaced limestone massif. The upper aqueduct is still in line with the rest of the aqueduct to the

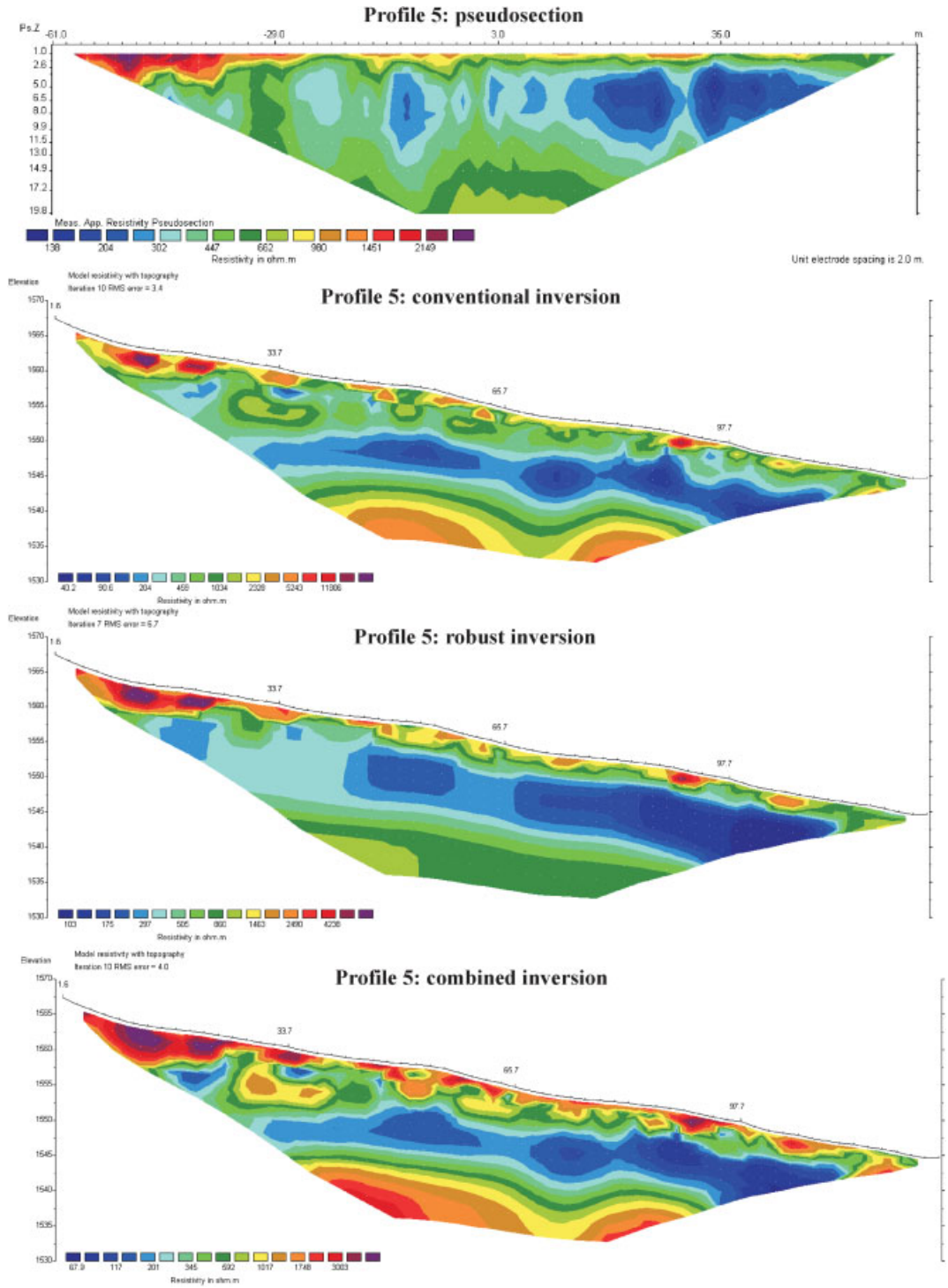

Plate 1. Measured apparent resistivity pseudosection and different computer inversion results (conventional, robust and combined) for profile 5. Inversion results take into account the topography. A best fit of colours is used for each profile individually, enabling a clear contrast of zones of different resistivity values. Comparison of the different models gives insight into which parts of the model are likely to correspond to the real geological structures, and which parts are strongly dependent on the inversion parameters.

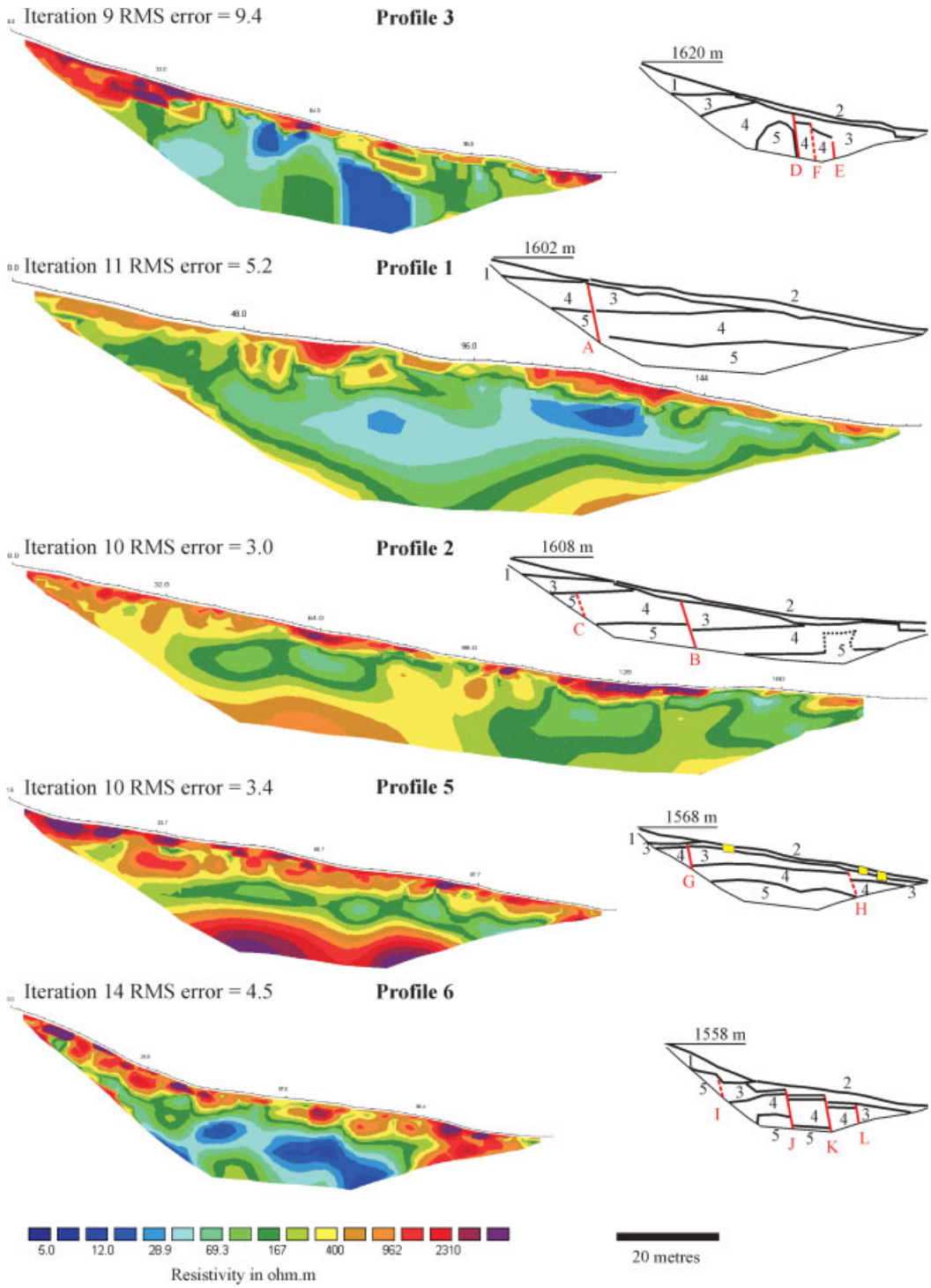

Plate 2. Two-dimensional resistivity profiles presented on the same scale and with the same colour scale. They represent the inversion results with the best visualization of the different characteristics discussed in the text. For profiles 2, 5 and 6 the conventional inversion was used. The combined inversion was used for profile 1 and the robust inversion with a robust data constraint was used for profile 3. The stratigraphical succession of the resistivity values is summarized for each profile on a half-scale proportion. Faults are indicated as red lines. Yellow boxes on profile 5 indicate the position of the archaeological test soundings.

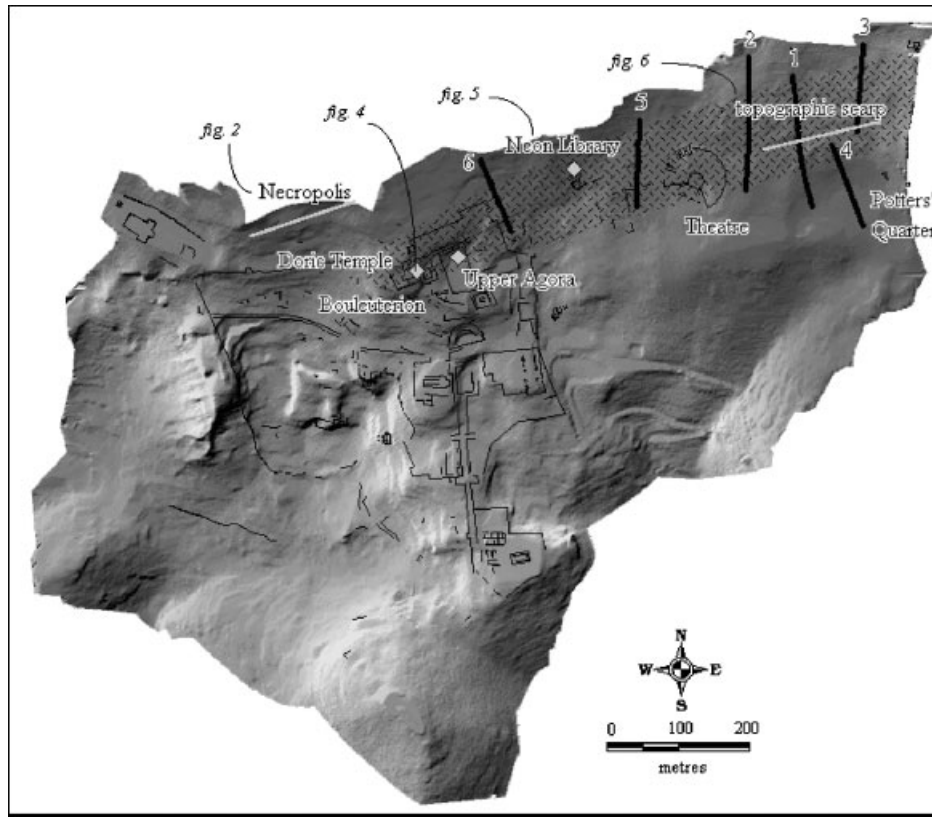

Figure 3. Overview map of the town of Sagalassos. The background is a shaded relief view from the digital elevation model (DEM) derived by digitizing the 1:500 scale topographic maps from the town (Depuydt, 2002). Features indicative of a fault are indicated in grey rectangles and lines (Figures 2, 4, 5 and 6). The hatched area delimits the assumed fault trace (after Sintubin *et al.*, 2003). The location of the two-dimensional resistivity profiles are indicated by numbered black lines.

east of Sagalassos and is less weathered than the lower one, suggesting that it was rebuilt after the faulting event. The rupture of the aqueduct, causing water shortage in the town, is considered to be related to a major earthquake at the beginning of the sixth century AD (Waelkens *et al.*, 2000). The displaced limestone massif fits in the active normal fault trace of the town (Sintubin *et al.*, 2003). However, the 7 m displacement is not likely to be the direct result of one single surface-rupturing event. It is more likely that fault reactivation, underneath the limestone massif, triggered it to slump (Sintubin *et al.*, 2003).

Data acquisition

In two-dimensional resistivity imaging, a spread of electrodes is laid out with a constant spacing along a straight line. Resistivity measurements are carried out using a specific electrode layout or array (e.g. the Wenner–Schlumberger array) that is best suited for the objectives of the study. For the selected array, different array separation factors (i.e. different values of the a and n parameters, see Figure 7) are chosen depending on the desired vertical resolution and penetration. For each array separation or 'data level', all possible measurements are carried out sequentially down the line of electrodes. In this way, a large number of independent apparent resistivity measurements are acquired, which need to be inverted to obtain a two-dimensional model of true subsurface resistivity. The resistivity measurements at Sagalassos were carried out with the LUND Imaging System from ABEM, which consists of four cables of 16 electrodes each, branched to a resistivity meter (Terrameter

Figure 4. Normal fault, filled with clay gouge, in the limestone bedrock of the Doric Temple (see Figure 3 for location). The continuation of the fault in the pavement of the Bouleuterion is not clear.

Figure 5. Normal faulting in the Neon Library (see Figure 3 for location).

Figure 6. View (westwards) of the topographic scarp, indicated by lines, to the east of the town (see Figure 3 for location).

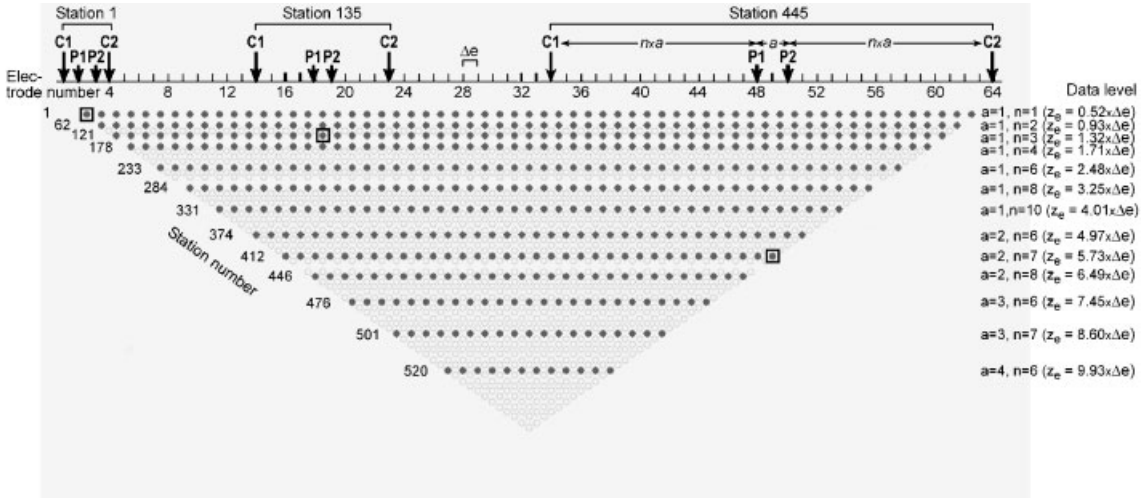

Figure 7. Arrangement of electrodes and sequence of measurements (here called 'stations') for the electrical tomography lines carried out at Sagalassos. We used a Wenner–Schlumberger (WSC) array with two current electrodes C1 and C2, and two potential electrodes P1 and P2. Δe is the constant electrode spacing along the line. The WSC array is determined by the separation factor a (the number of electrodes between P1 and P2) and n (the multiplication factor for the C1–P1 and P2–C2 separation). Note that the WSC array becomes an Wenner-alpha array if $n = 1$. For each data level the median depth of investigation, z_e, has been calculated following Edwards (1977).

Table 2. Relevant acquisition parameters for the two-dimensional resistivity profiles across the suspected fault trace

Profile number	Number of electrodes	Electrode spacing (m)	Layout	IP	Length (m)	Investigation depth (m)	Data quality
1	64	3	WSC	+	189	30	Resistivity: medium IP: bad
1b	64	3	DDP	−	189	22	Bad
2	96	2	WSC	+	190	20	Resistivity: medium IP: medium
3	64	2	WSC	−	126	20	Medium-poor
5	63	2	WSC	−	124	20	Excellent
6	64	1.8	WSC	−	113	18	Good

SAS-1000) through an electrode selector ES-464). Using a roll-along technique, the length of the profile can easily be extended by a multiple of 32 electrodes.

For the aim of this study, i.e. the detection of steeply dipping normal faults, two different electrode layouts were considered: the Wenner–Schlumberger (WSC) layout and the dipole–dipole (DDP) layout. The DDP layout is very sensitive to horizontal changes in resistivity, which could be expected across a normal fault, but is much less sensitive for vertical changes (e.g. subhorizontal layering). The WSC layout is moderately sensitive to both horizontal and vertical structures. Compared with DDP it has a larger depth of penetration and a better signal/noise ratio, but a narrower horizontal data coverage (Loke, 2001). The DDP layout has the additional disadvantage that it is more sensitive to off-axis structures, which can be a severe problem if the geology shows large variations lateral to the survey line. Both layouts were tested with otherwise identical parameters along profile 1 (WSC) and 1b (DDP). The DDP data appeared to be so noisy that they could not be inverted into a reliable model. The WSC layout proved to be the best compromise between horizontal and vertical resolution for the particular conditions at the site of Sagalassos. The electrode spacing along the survey line (i.e. the minimum inter-electrode spacing) was chosen to ensure the required resolution and penetration depth, and was a function of the position of the suspected fault along the profile and the space available. Profile 1 was laid out with a relatively large electrode spacing (3 m, corresponding to a median depth of investigation of 30 m for the deepest data level, see Figure 7), which confirmed that the bedrock depth did not exceed 10 m. From this profile, we concluded that a target depth of 20 m was sufficient, and subsequent profiles were carried out with an electrode spacing of 2 m.

Six profiles, totalling 870 m in length, were acquired. These profiles, except profile 4, were carried out perpendicular to the suspected fault trace (Figure 3). Profiles 1, 2 and 3 are located east of the Roman Theatre, profiles 5 and 6 east and west of the Neon Library, respectively. The elevation of the latter profiles is lower (30 m), but the slope is steeper. Profile 4 was carried out more to the south of the suspected fault trace across the central semicircular depression in the Potters' Quarter. The purpose of this profile was to gain a better understanding of the subsurface geometry of this depression, which is considered by Degryse *et al.* (2003) to be the result of a stepped open-quarrying system for the exploitation in historical times of weathering clays from the ophiolitic bedrock, used in the local pottery manufacture. This profile is beyond the scope of this paper and will not be discussed in detail. Table 2 summarizes all relevant acquisition parameters. The profiles are situated directly below the limestone front overlooking the town from the north, over a pile of coarse debris ('scree') shed from this cliff, characterized by slopes between 11° and 23°.

Along with resistivity, we also measured induced polarization (IP) in the time domain along profiles 1 and 2. In some cases, IP measurements can yield important additional information, i.e. presence of clay minerals and/or conductive minerals associated with the fault plane (Vanneste *et al.*, 2002). Unfortunately, the quality of the IP data was too poor (presence of a large number of negative values) to be inverted into a reliable two-dimensional model, and we therefore abandoned IP measurements for all other profiles.

Data processing

For each data point, the resistivity meter performs a stack of a minimum of two and a maximum of four measurements. The standard deviation for each stack is a good indicator of the quality of the data. Considering the difficult conditions, the quality of most profiles was relatively good, with standard deviations generally below 2.5%. The quality varied, however, considerably from profile to profile (Table 2). The best quality was attained for profiles 5 and 6, while profiles 1, 2 and 3 have a medium quality. As mentioned above, the quality of profile 1b, the only profile recorded with a DDP layout, was too poor to be further processed.

Before proceeding with the inversion, the data set was reduced: all negative resistivity values were rejected, as well as all data points with a standard deviation above a certain threshold (2.5% for profiles 5 and 6; 5% for profiles 1, 2 and 3). The filtered data were subsequently re-evaluated visually, and any remaining isolated extreme value was removed.

The measured resistivity values do not represent the true subsurface resistivity, but an 'apparent' resistivity, corresponding to the resistivity of a homogeneous subsurface that would produce the same resistance value for the given electrode arrangement (Loke and Barker, 1996). Pseudosections plotting the apparent resistivity as a point at the mid-point of the array against depth (e.g. median depth of investigation) do not give an accurate picture of the true subsurface resistivity, because these plots do not take into account that the signal of each value measured in fact originates from a volume of the subsurface that depends on the type of array used. Determining the true subsurface resistivity is an inverse problem. We inverted our data with the commercial RES2DINV software from GEOELECTRICAL. This program iteratively calculates a resistivity model section, trying to minimize the difference between the observed apparent resistivity values and those calculated from this model.

Several inversion methods were selected for each profile.

(i) The conventional smoothness-constrained least-squares method (also known as I_2-norm inversion method) gives optimal results where the subsurface geology shows a smooth variation, but tends to smear out the boundaries when sharp boundaries are present in the subsurface and to under- or overshoot the true resistivity values (Loke *et al.*, 2001).

(ii) The robust or blocky inversion method (I_1-norm inversion method) tends to produce internally homogeneous bodies with sharp boundaries, which can be more consistent with the geology in some cases.

(iii) The combined inversion method applies the smoothness-constrained inversion method and the ridge regression method. In situations with very-low-resistivity bodies, this method can sometimes correct for the large distortions of current paths just below such bodies.

The results of the different inversion methods vary from profile to profile. Comparison of the different models gives an insight into which parts of the model probably correspond to real geological structures, and which parts are strongly dependent on the inversion parameters (Plate 1). All inversions were carried out taking into account the topography along the profile.

Inversion results and resistivity stratigraphy

The stratigraphical succession of the resistivity values for each profile separately is summarized in Table 3. The profiles are discussed from top to bottom. All profiles show a similar stratigraphical succession (Plate 2).

Layer 1: a wedge-shaped, high-resistivity (>700 Ωm) surface layer is present in the upslope part of the profile. The toe of the wedge is orientated downslope.

Layer 2: downslope of layer 1, the surface layer is characterized by intermediate resistivities (200–1000 Ωm), in which small (2.5 by 5 m) high-resistivity (>1000 Ωm) bodies are embedded.

Layer 3: an intermediate resistivity (100–800 Ωm) layer that varies in thickness. It is often wedge-shaped with the toe downhill.

Table 3. Stratigraphical succession of the resistivity values for the two-dimensional resistivity profiles across the suspected fault trace. Description of the layers is from top to bottom

Profile	Attribute	Layer 1	Layer 2	Layer 3	Layer 4	Layer 5
1	**Shape**	Wedge	Surface layer with embedded bodies	Wedge	Horizontal/ continuous	Horizontal/ continuous
	Thickness (m)	0–8	5	1–7.5	12	>10
	Resistivity value (Ωm)	400–1000	200–500/>1000 for the bodies	100–500	25–85	>100
2	**Shape**	Wedge	Surface layer with embedded bodies	Wedge	Horizontal /continuous	Horizontal /continuous
	Thickness (m)	0–7.5	5	0–10	10	>7.5
	Resistivity value (Ωm)	900–1000	400–500/>3000 for the bodies	400–450	85–260	>400
3	**Shape**	Wedge	Surface layer with embedded bodies	Lower edges of the profile	Central zone of the profile	Vertical orientated zone
	Thickness (m)	0–10	2.5	0–12	>18	>18
	Resistivity value (Ωm)	1000–3000	400–1000/>1000 for the bodies	100–500	15–85	100–200
5	**Shape**	Wedge	Surface layer with embedded bodies	Wedge	Horizontal /continuous	Horizontal /continuous
	Thickness (m)	0–7	2.5	1–8	7.5	>7.5
	Resistivity value (Ωm)	>2000	1000–2000/>3000 for the bodies	400–1000	135–500	800–1200
6	**Shape**	Wedge with embedded bodies	Surface layer with embedded bodies	Small delimited area	Horizontal /continuous	Small delimited area
	Thickness (m)	0–6	5–10	7.5	>13	>6
	Resistivity value (Ωm)	1000–3000/ >3000 for the bodies	400–900/ >3000 for the bodies	100–200	25–60	100–200

Layer 4: a continuous, more or less horizontal layer with relatively low resistivity (15–500 Ωm).

Layer 5: at the bottom of most profiles, resistivities rise again up to 2000 Ωm. The average resistivity, however, is lower (400 Ωm). Dome-like structures, reaching into layer 4, can be observed on profiles 2, 3 and 6.

Interpretation

Layers 1 and 2

The resistivity values from layers 1 and 2 can be correlated with surface observations. Most profiles start close to the steep limestone cliff situated at the northern extremity of the town. Therefore, these profiles are situated at the southern tip of the young scree deposits coming from this steep limestone cliff (Figure 8). These screes consist of small limestone fragments (clasts). The space between the clasts is not filled in the upper parts of the scree tongue, but some loose ground infill exists in the lower part. The first electrodes were often located in these screes. Moreover, in the case of profile 5, the first electrode did not make measurements because the contact between this electrode and the subsurface was not good. The air between the clasts probably gave an infinite resistivity value. Therefore, the scree deposits give high-resistivity values because bad conductivity exists between the limestone clasts. This is observed in the upper parts of most resistivity profiles (Plate 2). Moreover, the scree deposits are characterized by a wedge shape (Librecht *et al.*, 2000). Layer 1 (Plate 2) is thus interpreted as young scree deposits at the base of the steep limestone cliff. At profile 3, this scree was visible in the field and reached as far as electrode number 23. On the resistivity profile it is also clear that the tip of the wedge-shaped,

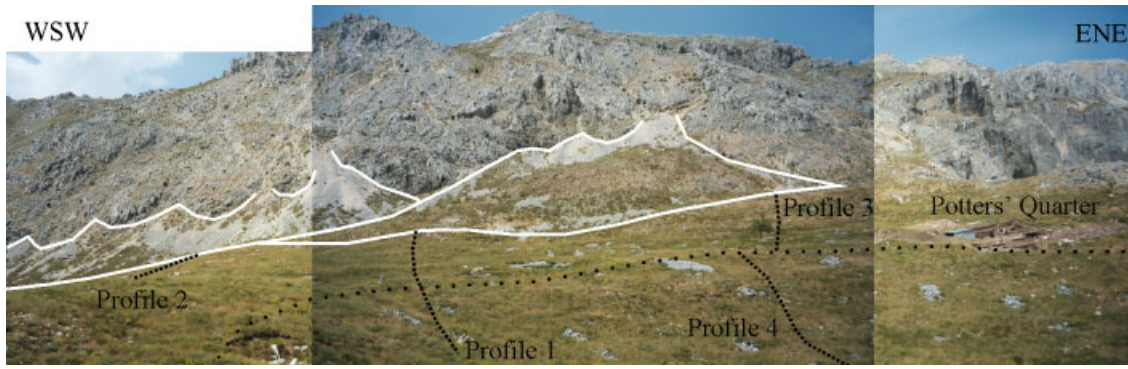

Figure 8. Screes originating from the limestone front, reaching the upper parts of the resistivity profiles.

high-resistivity body of layer 1 reaches exactly up to electrode number 23 (Plate 2).

In the area where the resistivity profiles were measured, many archaeological structures and/or piled rocky blocks are present at the surface. Tombs, monumental structures and anthropogenic terraces were identified in this area (Martens *et al.*, in press). In nearly all cases where archaeological structures were visible at the surface, an embedded high-resistivity body is observed in resistivity layer 2. It is therefore fair to assume that all other embedded high-resistivity bodies also correspond to archaeological structures. As building remains consist of large limestone blocks (ashlars), the space between the different building stones will result in very high-resistivity values. In this way, embedded high-resistivity bodies probably indicate the presence of different archaeological structures not visible at the surface. Other examples of such embedded high-resistivity bodies are described in Griffiths and Barker (1994) and Kampke (1999). The former authors have interpreted them as shallow slab-like bodies of limited extent corresponding to a roadway or paved walk. In the case described by Kampke (1999), the high-resistivity bodies represent a Roman foundation wall and a hypocaust system.

Layers 2 and 3

The resistivity values from layers 2 and 3 can be correlated with observations made in trenches of archaeological excavations between the Neon Library and the Roman Theatre. These archaeological excavations enable the study of the top 3 m of the surface layer. Different archaeological test soundings (TSW1–4 and TSN) were carried out during the 1999 and 2000 field campaigns in the area of profile 5 (Figure 9) (Waelkens *et al.*, in press). All these excavations display a similar lithostratigraphical succession, with different archaeological and colluvial layers. However, this lithostratigraphical succession (divided up to six layers) is too detailed for the resolution of the resistivity profiles. In general, the excavated material consists of a sandy to silty loose soil, which is gravelly owing to the abundant presence of (lime)stone blocks of different sizes. The soil, moreover, contains charcoal and mortar fragments, and a large amount of archaeological finds (ceramics, bone, glass, metal, stucco fragments, terracotta objects, piped water channels, etc.) (Figure 10). Within these archaeological layers, remains of an ancient street pattern were found. Many walls of buildings along this street pattern are still visible at the surface. The whole area is covered by colluvial material coming from the slopes. Therefore, the surface layer should be approximately the same for the areas that were excavated and the areas where the other resistivity profiles were measured. The only lateral variation is the concentration of archaeological material that is dependent on the proximity of archaeological structures. This surface layer corresponds to layer 2 of the resistivity profiles. We can conclude that the colluvial material, observed in the archaeological test soundings, corresponds with the intermediate-resistivity layer 2, in which small high-resistivity bodies are embedded. However, the base of the archaeological soundings near profile 5 are all

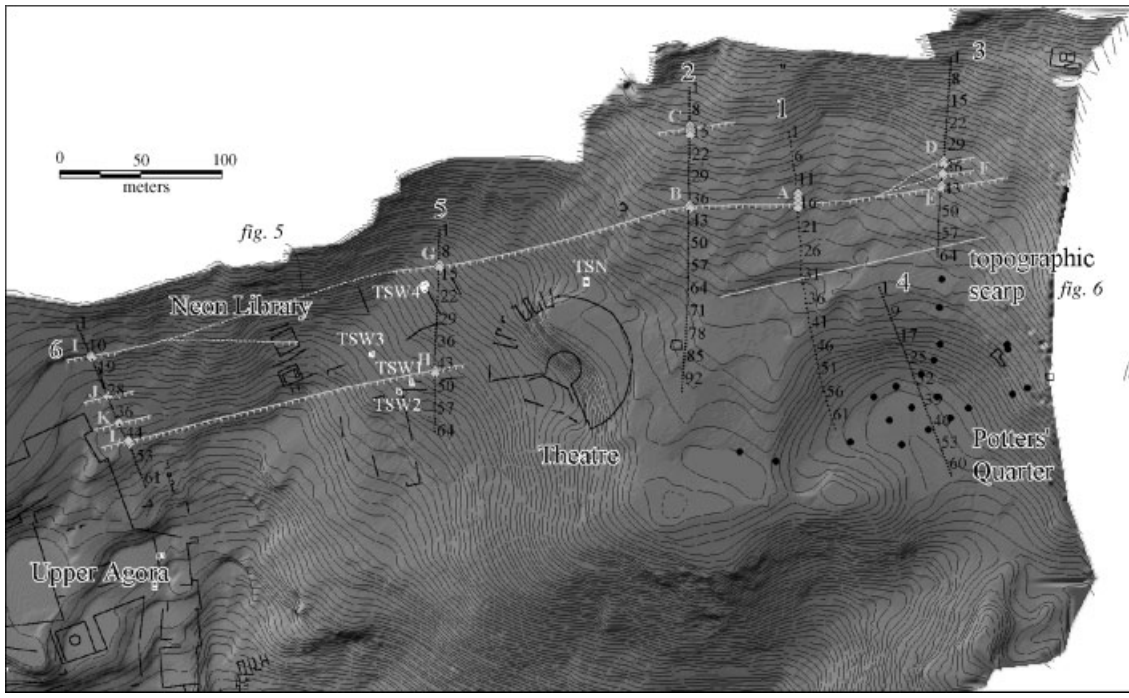

Figure 9. Area covering the two-dimensional resistivity measurements with indication of the profiles (the small black dots indicate the electrodes position), fault locations (grey rectangles), fault correlations, archaeological structures, archaeological test soundings (white boxes) and boreholes (black dots). The contour interval is 1 m.

near the transition of layers 2 and 3 (Plate 2). Only in sounding TSW2 (the deepest sounding), has part of layer 3 been excavated. The part corresponding with resistivity layer 3 is described as a compact silty to loamy, orange-brown to yellowish-brown soil, containing small- to medium-sized stones and numerous small-sized charcoal fragments. There is a marked decrease in the quantity of archaeological finds with depth, until the soil ceased to contain any archaeological relics. The ceramics of this layer belong to the early Imperial period (layer 5 of sounding TSW2 in Martens *et al.*, 2000).

These observations can be interpreted in terms of resistivity values. The archaeological layers above layer 5 of sounding TSW2 consist of a loose soil with the inclusion of different limestone fragments resulting in an intermediate resistivity value (layer 2). The conductivity in this layer is better than where the limestone fragments are not connected with loose soil, as for the screes (layer 1). On the other hand, conductivity is lower than in a normal soil profile because the limestone fragments have a higher resistivity. The lower resistivity of layer 3 is probably due to the fact that this layer is better compacted (less air) and contains less archaeological material. The corresponding archaeological layer is interpreted as a pre-Roman layer into which the foundations of an Augustan (25 BC to AD 14) building were dug (Martens, personal communication, 2003). Layer 3 is thus interpreted as older (pre-occupation) slope deposits.

Layers 4 and 5

The archaeological excavations and a test sounding on the Upper Agora indicate that its bedrock consists of a weathered ophiolitic mélange (Degryse, personal communication, 2003). The southern end of profile 6 is 90 m to the northeast of the Upper Agora and only 6 m higher (Figures 3 and 9). As layer 4 in profile 6 is interpreted to have been displaced by a normal fault (see further) it is possible to correlate the weathered ophiolitic bedrock forming the substrate of the Upper Agora with layer 4 of profile 6.

Figure 10. Sandy to silty loose soil with limestone clasts in archaeological test soundings. This corresponds to resistivity layer 2.

Layer 4 in the profiles to the east of the Roman Theatre can be interpreted thanks to profile 4 in the Potters' Quarter, which is approximately the continuation of profile 1. In the framework of an interdisciplinary study of the local potter's craft at Sagalassos a series of boreholes was drilled in the Potters' Quarter (Degryse *et al.*, 2003) (Figure 9). The soil sequence in that area consists of (Degryse *et al.*, 2003):

(i) the most recent colluvial layer; it has a sandy, clay or loam texture; the structure is granular and angular blocky; pores and roots are abundant; it is extremely calcareous with abundant limestone fragments and contains pottery waste; the thickness of this layer seems to change, between 140 to over 300 cm, from place to place around the Potters' Quarter; this reflects the influence of the topography;
(ii) a yellow-brown layer with a clay or loam texture; the structure is subangular blocky; pores and roots are abundant; it is extremely calcareous;
(iii) a red, clay-rich weathered horizon (Bss horizon) developed from the ophiolitic bedrock with vertic properties;
(iv) weathered ophiolitic bedrock.

This soil sequence is considered to have formed in four phases (Degryse *et al.*, 2003). Firstly, the ophiolitic bedrock weathered. Weathering was so intense that vertic properties developed, resulting in the Bss horizon. Secondly, the forest clearing in the Potters' Quarter from ca. 800–510 BC until ca. 400–210 BC (Vermoere *et al.*, 2002) may have initiated soil erosion with consequent removal of the upper part of the vertisol section, which colluviated downslope. This resulted in the yellow-brown layer. Thirdly, human activity often resulted in the removal of both layers for use in the pottery industry. In the last phase, a recent colluvial layer covered the area.

From its characteristics, it is clear that the top layer corresponds to layer 2 in the resistivity profiles. This colluvial material corresponds with the intermediate resistivity values of the resistivity profiles. It is the same colluvial material as observed in the archaeological soundings near profile 5. From the correlation between profile 4 and the boreholes along it (Figure 9), layer 4 in the resistivity profiles corresponds to weathered ophiolitic bedrock. A correlation of the southern end of profile 1 with the northern end of profile 4 (Figure 9) shows that layer 4 of profile 1 can be interpreted as weathered ophiolitic bedrock.

A clear difference in lithology exists under the top layer between the boreholes within the Potters' Quarter depression and those on the plateau to the west. In boreholes more to the west, the bedrock consists of limestone and the weathering products of that limestone are found under the colluvial layers. So, either limestone or weathered ophiolitic bedrock is present under the colluvial layers in the vicinity of the resistivity profiles. It is expected that limestone and weathered ophiolitic bedrock would give distinctively different resistivity values. Limestones have resistivity values between 50 and a few thousand Ωm and weathered mafic magmatic rocks have resistivity values between 5 and 50 Ωm. Layers 4

and 5 in the adjacent profiles 2 and 5 have clearly higher resistivity values than in the other profiles (Table 3 and Plate 2). In profiles 1, 3 and 6 layer 4 does not reach over 85 Ωm, whereas in profiles 2 and 5 layer 4 has similar resistivity values as layer 5 of profiles 1, 3 and 6. As discussed above, ophiolitic bedrock is likely to occur in profiles 1, 3, 4 and 6. In addition, the resistivity values of layer 4 in these profiles correspond with those for weathered mafic magmatic rocks. Layers 4 and 5 of profiles 2 and 5 thus could be interpreted as, respectively, the weathered top of limestone bedrock and unweathered limestone bedrock. In addition, the resistivity values of these layers correspond with those for limestone. However, as no boreholes are located along these resistivity profiles, conclusive proof is missing. In the centre of profile 3, a dome-like structure can be observed within layer 5 (Plate 2). Similar features are observed in profiles 4 and 6 (Plate 2). These structures display higher resistivity and seem to 'intrude' in layer 4. The difference in resistivity values could be caused by different characteristics of the weathered ophiolitic bedrock. The origin of these structures is yet unknown.

In both profiles to the west and east of the Roman Theatre, layer 4 is interpreted as weathered bedrock. In the resistivity profiles, layer 4 displays a horizontal layering. However, there is a significant difference in elevation between the profiles to the west and east of the Roman Theatre. Yet, the same weathered bedrock layers are present regardless of the fact that they seem to be horizontal on the resistivity profiles. The most plausible explanation is that layer 4 is following the topography. This would be characteristic for the weathered top of a bedrock. In this case, layer 5 (no borehole data) represents the unweathered ophiolitic or limestone bedrock and layer 4 represents the weathered top of this bedrock. The low-resistivity values of layer 4 can be the result of more clay resulting from weathering processes or the presence of the water table above impermeable unweathered ophiolitic bedrock (Degryse *et al.*, 2003). The variation in thickness of layer 4, between 7.5 and 12 m, can be the result of different degrees of weathering. Weathering must have been severe as layer 4 reaches a thickness of up to 12 m.

Features indicative of normal faulting

On profile 1 there are indications for only one fault, i.e. in the upslope part of the profile (Plate 2). Fault A is located at the upslope termination of layer 4 and at the juxtaposition of the wedge-shaped layer 3 downslope against the bedrock (layer 5?) upslope. The scarp, earlier suspected to be a fault scarp (Sintubin *et al.*, 2003) in the centre of the profile, does not correspond with a fault at depth.

A strong indication exists on profile 2 for a fault in the centre of the profile, and possibly a second fault in the upslope part (Plate 2). Fault B shows a clear displacement of layer 4 and the juxtaposition of the wedge-shaped layer 3 (downslope) against layer 4 (upslope). However, layer 2 becomes thinner downslope of the suspected fault. Fault C is located at the upslope termination of layer 4 (observed in all inversions), and probably also of the wedge-shaped layer 3.

Profile 3 displays strong indications for a main fault in the centre of the profile, and for at least one additional fault downslope (Plate 2). Fault D has a clear displacement of layer 4 and juxtaposes layers 3 and 4 downslope against layers 4 and 5 upslope. Fault E displaces layer 4 to below the bottom of the profile and a thickening of layer 3 occurs downslope of the fault. A possible small displacement of the top of layer 4 and the base of layer 3, in between faults D and E, could be indicative of a fault F. Layer 2 does not show any clear displacement on all of these faults. Only at the downslope extremity of the profile does this layer become significantly thicker (also the case on profile 2), but the limited depth range of the profile does not allow verification of whether there is any displacement at depth. Most likely this corresponds to a filled depression.

Both combined and conventional inversions of profile 5 show good evidence of a fault in the upslope part of the profile (Plates 1 and 2). Fault G shows a clear displacement of layer 4 and the juxtaposition of the wedge-shaped layer 3 (downslope) against layer 4 (upslope) in the upslope part of the profile. There is an indication of a second fault (fault H), displacing layers 3 and 4, near the downslope extremity of the profile. The robust inversion (Plate 1) does not

show any fault on this profile, but we suspect that this inversion did not catch the heterogeneity close to the extremity of the profile.

Profile 6 shows evidence of several faults in the centre and downslope part of the profile (Plate 2). Faults J, K and L show clear displacement of layer 4 in three successive steps and layers 2 and 3 thicken downslope. There is a hint of an additional fault (fault I) near the upslope extremity of the profile, which seems to juxtapose the wedge-shaped layer 3 downslope against the bedrock upslope, and maybe even affects layer 1. This seems to be the only profile where layer 2 is affected by faulting.

Some features that occur systematically on most profiles are indicative of the presence of normal faults. The clear vertical displacements, up to 10 m, of the top of layer 4 are considered evidence for south-dipping normal faults. In some cases the displacement of the bottom of this layer also can be observed. The overlying wedge-shaped layer 3 displays a sharp limit at this fault contact and also shows a clear vertical displacement. The 'older slope debris layer' (layer 3) seems to have the geometry of a colluvial wedge. This is indicative of the presence of a fault scarp, and thus a surface rupture. Layers 1 and 2 are not affected, with the possible exception of profile 6.

In most cases, more than one fault could be observed in the profiles (Plate 2 and Figure 9). In profile 1, fault A displays an offset of the top of the bedrock of at least 10 m. Faults B and C in profile 2 display both an offset of 10 m. In profile 3, fault D shows a 5 m offset, fault E at least 10 m and fault F 2 m. In profile 5, fault G has an 8 m offset and fault H 3 m. The offset of fault I in profile 6 cannot be defined. Fault J in profile 6 displays a 2 m offset, fault K 2 m and fault L 7 m. The total fault displacement varies from place to place. This can be due to the fact that not all the profiles represent the whole width of the fault zone.

Fault correlation

An attempt has been made to correlate the different faults observed in each profile (Figure 9). Between profiles 1, 2 and 3, to the east of the Roman Theatre, a correlation is obvious. Faults A and B and the fault zone D–E–F have the same offset and thus can be correlated. They are therefore considered to represent the main fault. Fault G of profile 5 and I of profile 6, to the west of the Roman Theatre, could be correlated because the location and characteristics of layer 3 are similar. The other, smaller faults (J and K) are restricted to one profile and are probably secondary bifurcations of the main fault. They most probably die out laterally. Fault H of profile 5 and fault L of profile 6 could represent the same fault. This fault lies at the border of a topographic scarp on the DEM that could represent its surface expression (Figure 9). The offset is, however, not the same (smaller offset on fault H), but could be due to the disappearance of this fault to the east.

Correlation of the profiles east and west of the Roman Theatre is more difficult as they lie at a greater distance and different elevation. On the scale we are working on, topographical effects on the position of the fault trace can, however, be neglected. Although the elevation difference of the trace of the main fault between profiles 2 (1590 m) and 5 (1560 m) is 30 m, the deviation of a straight fault trace would be only 11 m (assuming a fault dip of 70°). The main fault of profiles 1, 2 and 3 could be correlated with fault G of profile 5 as location and fault offset are similar. The fault trace mapped is aligned following a N80°E trend, parallel to the limestone front and the faults running through the mosaic floor of the Neon Library (Waelkens *et al.*, 2000). The fault trace inferred, however, does not correspond to a straight line. We therefore have to assume that the fault planes show local changes in trend.

Discussion

The two-dimensional resistivity profiles show good evidence for the presence of an active normal fault zone that passes underneath ancient Sagalassos. This is indicated by the displacement of the bedrock and overlying colluvium that is systematically observed on all the profiles. The correlation of the observed faults between the different profiles is distinct.

As large-scale rotational slumps occur in and around ancient Sagalassos (Verstraeten *et al.*, 2000), one could argue that the faults observed on the resistivity profiles represent the sliding surface of such rotational slumps. The displacements on some of the observed faults are indeed similar to that observed at the displaced aqueduct (see earlier). Although the depth range of our profiles is probably not large enough to distinguish between tectonic normal faults and the sliding surface of such rotational slumps, the following arguments favour a tectonic interpretation of the observed displacements. The detected fault on the resistivity profiles represents a rather linear fault trace over a distance of at least 550 m. In the case of a slump we would expect a more curved (concave) fault trace. Moreover, such a large-scale rotational slump would have a clear geomorphological expression, which is not the case (Figure 3). In addition, no back-tilt of the bedrock, typical within a slumped massif, has been observed on the resistivity profiles. Thus, the detected displacements in the resistivity profiles are interpreted as the main active normal fault of which the degraded fault plane corresponds to the limestone range north of Sagalassos. The large displacement on some faults, however, cannot be the result of one single seismic event. It is more likely that layer 3 consists of several small colluvial wedges that are representative of different earthquakes. The resolution of two-dimensional resistivity does not allow the visualisation of such colluvial wedges within layer 3.

Moreover, the displacement of debris layer 3 implies an *active* normal fault. This indicates that the fault has been reactivated after the deposition of this debris layer. According to Degryse (personal communication, 2003), the excavated material of layer 3, from the archaeological sounding near profile 5, could correspond to the debris layer that is thought to have been deposited after the forest clearing in the Potters' Quarter from ca. 800–510 BC until ca. 400–210 BC (Vermoere *et al.*, 2002; Degryse *et al.*, 2003) and prior to the construction of the buildings of which the remains are observed in the resistivity profiles.

Two features indicate that a reactivation of this fault also may have occurred during the occupation of the town. The displaced aqueduct east of the town and subsequent water shortage at Sagalassos demonstrates the occurrence of a seismic event in the sixth century AD (Waelkens *et al.*, 2000). The faulted Neon Library indicates surface rupture during an earthquake in the middle of the seventh century AD (Waelkens *et al.*, 2000). In addition, there are indications of displacement of layers 1 and 2 on profile 6. Between faults H and L on the resistivity profiles a topographic scarp can be interpreted as a fault scarp (Figure 9). No other topographic scarps along the resistivity profiles correspond to the location of the faults identified. Most of them probably correspond to anthropogenic terrace walls. Because of the lack of any prominent topographic fault scarp, a reactivation of this fault segment during the sixth and seventh centuries AD can be questioned. A possible explanation is that the surface displacement was only a few centimetres (cf. the Neon Library) during those events and that the fault scarp degradation, and the burial by recent screes from the limestone front, rapidly erased any trace of the seismic event so that only in a building, such as the Neon Library, the trace of this event was preserved. However, it is not likely that this would represent the total offset because the main faults on the resistivity profiles do not occur laterally of the Neon Library.

Sagalassos has thus been built in the hanging wall of an active normal fault (Figure 11). Other cases of faults passing underneath ancient cities are known (Hancock and Altunel, 1997; Marco *et al.*, 1997; Altunel, 1998; Galadini and Galli, 1999; Akyüz, 2001; Galli and Galadini, 2001; Pavlides *et al.*, 2001; Altunel *et al.*, 2003). The cases of Priene in southwest Turkey (Altunel, 1998), Hierapolis in western Turkey (Hancock and Altunel, 1997) and Knidos in southwest Turkey (Altunel *et al.*, 2003) are similar to Sagalassos. These cities were also built in the hanging wall of an active normal fault. In the eastern Mediterranean region active normal faults are often characterized by a steep fault scarp within limestone. This limestone ridge (degraded fault plane) forms an ideal natural defence to one part of a town. However, this resulted in building the town on top of an active fault that could generate devastating earthquakes.

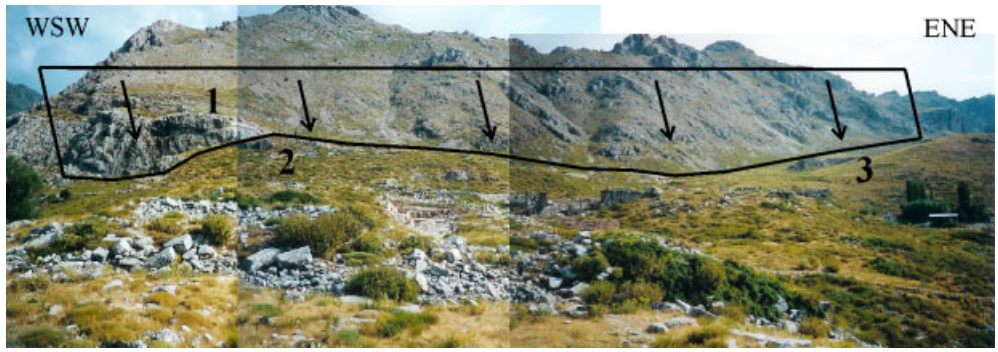

Figure 11. Sagalassos was most likely built in the hanging wall of an active normal fault. The Necropolis (1), Bouleuterion and Upper Agora (2) and Theatre (3) are indicated.

Conclusions

In spite of the rather rough terrain conditions, two-dimensional resistivity imaging enabled us to infer the presence of an active normal fault at Sagalassos and thus corroborates the previous findings based on surface data (Similox-Tohon *et al.*, 2002; Sintubin *et al.*, 2003). In addition, two-dimensional resistivity imaging enables the visualization of different archaeological structures in the subsurface that are not visible at the surface. The precise location of the suspected fault trace could be identified. Sagalassos has been built on an active normal fault, most probably owing to the favourable geomorphological situation linked with such a fault. Eventually this fault could have reactivated, causing serious damage to the town. Sagalassos was abandoned around the middle of the seventh century AD after a devastating earthquake, possibly on this fault.

Acknowledgments

We would like to thank an anonymous referee for the constructive review of the manuscript, T. Camelbeeck for stimulating discussions on the geophysical methods, F. Martens and P. Degryse for their constructive comments on the stratigraphy and J. Poblome for the logistical support in the field. This research is supported by a Concerted Action of the Flemisch Government (GOA 02/2) and the Belgian Programme on Interuniversity Poles of Attraction initiated by the Belgian State, Prime Minister's Office, Science Policy Programming (IUAP P5/09). M. Sintubin is Research Associate of the Onderzoeksfonds at the K.U. Leuven. M. Waelkens is L. Baert-Hofman Professor in Eastern Mediterranean Archaeology.

References

Akyüz HS. 2001. Geological and archaeological evidence for post-Roman earthquake surface faulting at Cibyra, SW Turkey. *Geodinamica Acta* **14**: 95–101.

Altunel E. 1998. Evidence for damaging historical earthquakes at Priene, Western Turkey. *Turkish Journal of Earth Sciences* **7**: 25–35.

Altunel E, Barka AA, Akyüz HS. 1999. Palaeoseismicity of the Dinar fault, SW Turkey. *Terra Nova* **11**: 297–302.

Altunel E, Stewart IS, Barka AA, Piccardi L. 2003. Earthquake faulting at ancient Cnidus, SW Turkey. *Turkish Journal of Earth Sciences* **12**: 137–151.

Ambraseys NN. 2001. Reassessment of earthquakes, 1900–1999, in the Eastern Mediterranean and the Middle East. *Geophysical Journal International* **145**: 471–485.

Ambraseys NN, Jackson JA. 1998. Faulting associated with historical and recent earthquakes in the Eastern Mediterranean region. *Geophysical Journal International* **133**: 390–406.

Barka AA, Reilinger R, Saroglu F, Sengör AMC. 1995. The Isparta Angle: its importance in the neotectonics of the Eastern Mediterranean Region. In *International Earth Sciences Colloqium on the Aegean Region*, 9–14 October, Vol. 1: 3–17.

Bozkurt E. 2001. Neotectonics of Turkey—a synthesis. *Geodinamica Acta* **14**: 3–30.

Degryse P, Poblome J, Donners K, Deckers J, Waelkens M. 2003. Geoarchaeological investigations of the 'Potters' Quarter' at Sagalassos, southwest Turkey. *Geoarchaeology* **18**(2): 255–281.

Degryse P, Muchez P, Sintubin M, Clijsters A, Viaene W, Dederen M, Schrooten P, Waelkens M. In press. Geological mapping of the area

around Sagalassos (SW Turkey). In *Sagalassos VI. Report on the Survey and Excavation Campaigns of 1998, 1999, 2000 and 2001*, Waelkens M, Poblome J (eds). Acta Archaeologica Lovaniensia Monographiae: University Press, Leuven.

Demanet D, Renardy F, Vanneste K, Jongmans D, Camelbeeck T, Meghraoui M. 2001. The use of geophysical prospecting for imaging active faults in the Roer Graben, Belgium. *Geophysics* **66**(1): 78–89.

Depuydt F. 2002. *Topographical Map of Sagalassos*. Cartographical Department, K.U. Leuven, scale 1:500.

Edwards LS. 1977. A modified pseudosection for resistivity and induced-polarization. *Geophysics* **42**: 1020–1036.

Eyidogan H, Barka AA. 1996. The 1 October 1995 Dinar earthquake, SW Turkey. *Terra Nova* **8**: 479–485.

Galadini F, Galli P. 1999. Palaeoseismology related to the displaced Roman archaeological remains at Egna (Adige Valley, northern Italy). *Tectonophysics* **308**: 171–191.

Galli P, Galadini F. 2001. Surface faulting of archaeological relics. A review of case histories from the Dead Sea to the Alps. *Tectonophysics* **335**: 291–312.

Goldsworthy M, Jackson J. 2000. Active normal fault evolution in Greece revealed by geomorphology and drainage patterns. *Journal of the Geological Society, London* **157**: 967–981.

Griffiths DH, Barker RD. 1994. Electrical imaging in archaeology. *Journal of Archaeological Science* **21**(2): 153–158.

Guidoboni E, Comastri A, Traina G. 1994. *Catalogue of Ancient Earthquakes in the Mediterranean Area up to the 10th Century*. Instituto Nazionale di Geofisica: Roma.

Hancock PL, Altunel E. 1997. Faulted archaeological relics at Hierapolis (Pamukkale), Turkey. In *Paleoseismology: Understanding past earthquakes using Quaternary Geology*, Hancock PL, Michetti AM (eds). *Journal of Geodynamics* **24**: 21–36.

Kampke A. 1999. Focused imaging of electrical resistivity data in archaeological prospecting. *Journal of Applied Geophysics* **41**: 215–227.

KOERI. 2002. Kandili Observatory and Earthquake Research Institute earthquake catalogue. http://www.koeri.boun.edu.tr/jeofizik/mapeng.htm (accessed September 2002).

Koral H. 2000. Surface rupture and rupture mechanism of the October 1, 1995 ($M_w = 6.2$) Dinar earthquake, SW Turkey. *Tectonophysics* **327**: 15–24.

Librecht I, Paulissen E, Verstraeten G, Waelkens M. 2000. Implications of environmental changes on slope evolution near Sagalassos. In *Sagalassos V. Report on the Survey and Excavation Campaigns of 1996 and 1997*, Waelkens M, Loots L (eds). Acta Archaeologica Lovaniensia Monographiae 11: University Press, Leuven; 799–817.

Loke MH. 2001. *Tutorial: 2-D and 3-D Electrical Imaging Surveys*. Geotomo Software: Penang, Malaysia.

Loke MH, Barker RD. 1996. Rapid last-squares inversion of apparent resistivity pseudosections by a quasi Newton method. *Geophysical Prospecting* **44**: 131–152.

Loke MH, Acworth I, Dahlin T. 2001. A comparision of smooth and blocky inversion methods in 2-D electrical imaging surveys. In *Australian Society of Exploration Geophysicists 15th Geophysical Conference and Exhibition*, Brisbane, August; 4.

Marco S, Agnon A, Ellenblum R, Eidelman A, Basson U, Boas A. 1997. 817-year-old walls offset sinistrally 2.1 m by the Dead Sea Transform, Israel. In *Paleoseismology: Understanding past earthquakes using Quaternary Geology*, Hancock PL, Michetti AM (eds). *Journal of Geodynamics* **24**: 11–20.

Martens F, Zaman E, De Simone R. 2000. Unpublished report of the 2000 street soundings. Sagalassos Archaeological Research Project: K.U. Leuven; 153–171.

Martens F, Waelkens M, Poblome J, Degeest R, Vanhaverbeke H. In press. The first three seasons of intensive urban survey at Sagalassos (1999–2001): a chronological, spatial and functional analysis of the occupation pattern of the urban area. In *Sagalassos VI. Report on the survey and excavation campaigns of 1998, 1999, 2000 and 2001*, Waelkens M, Poblome J (eds). Acta Archaeologica Monographiae Lovaniensia: University Press, Leuven.

Noel M, Xu B. 1991. Archaeological investigation by electrical resistivity tomography: a preliminary study. *Geophysical Journal International* **107**: 95–102.

Pavlides SB, Kociu S, Mukelli P, Hyseni A, Zouros N. 2001. Neotectonics of the Southwestern Albania and archeological evidence for seismic activity in Butrinti. In *4th International Symposium on Eastern Mediterranean Geology*, Isparta, Turkey, 21–25 May; 36.

Pellerin L. 2002. Applications of electrical and electromagnetic methods for environmental and geotechnical investigations. *Surveys in Geophysics* **23**: 101–132.

Poisson A. 1977. *Recherches géologiques dans les Taurides occidentales (Turquie)*. Thèse doctorat d'Etat, Université Paris-Sud.

Price SP, Scott B. 1994. Fault-block rotations at the edge of a zone of continental extension: southwest Turkey. *Journal of Structural Geology* **16**(3): 381–392.

Sambuelli L, Socco LV, Brecciaroli L. 1999. Acquisition and processing of electric, magnetic and GPR data on a Roman site (Victimulae, Salussola, Biella). *Journal of Applied Geophysics* **41**: 189–204.

Similox-Tohon D, Sintubin M, Fernandez M, Muchez P, Waelkens M. 2002. Active normal

faults near the ancient city of Sagalassos (SW Turkey) revealed by geomorphological features and drainage patterns using satellite images and a digital elevation model. In *Environmental Catastrophes and Recovery in the Holocene*, Abstracts Volume, Leroy S, Stewart IS (eds). Brunel University, West London (UK), 28 August–2 September; 78–79.

Similox-Tohon D, Sintubin M, Muchez P, Waelkens M. 2003. In search of fault(s) responsible for the historical earthquakes at the ancient city of Sagalassos (SW Turkey). In *Tectonic Studies Group*, Abstracts Volume, University of Liverpool (UK), 8–10 January.

Sintubin M, Muchez P, Similox-Tohon D, Verhaert G, Paulissen E, Waelkens M. 2003. Seismic catastrophes at the ancient city of Sagalassos (SW Turkey) and their implications for the seismotectonics in the Burdur-Isparta area. *Geological Journal* **38**: 1–16.

Steegen A, Cauwenberghs K, Govers G, Waelkens M, Owens EJ, Desmet P. 2000. The water supply to Sagalassos. In *Sagalassos V. Report on the Survey and Excavation Campaigns of 1996 and 1997*, Waelkens M, Loots L (eds). Acta Archaeologica Lovaniensia Monographiae 11: University Press, Leuven; 635–649.

Stiros SC, Jones RE. 1996. *Archaeoseismology*. Fitch Laboratory Occasional Paper 7, Whitbread IK (ed). Institute of Geology and Mineral Exploration and The British School at Athens: Athens; 268.

Taymaz T, Price S. 1992. The 1971 May 12 Burdur earthquake sequence, SW Turkey: a synthesis of seismological observations. *Geophysical Journal International* **108**: 589–603.

Thacker PT, Ellwood BB, Pereira CMC. 2002. Detecting Palaeolithic activity areas through electrical resistivity survey: an assessment from Vale de Obidos, Portugal. *Journal of Archaeological Science* **29**(6): 563–570.

Vanneste K, Verbeeck K, Camelbeeck T. 2002. Exploring the Belgian Maas valley between Neeroeteren and Bichterweert for evidence of active faulting. In *Proceedings, First Geologica Belgica International Meeting*, Leuven, 11–15 September. Aardkundige Mededelingen; **12**: 5–8.

Vermoere M, Bottema S, Vanhecke L, Paulissen E, Waelkens M, Smets E. 2002. Palynological evidence for late Holocene human occupation recorded in two wetlands in southwest Turkey. *The Holocene* **12**(5): 569–584.

Verstraeten G, Paulissen E, Librecht I, Waelkens M. 2000. Limestone platforms around Sagalassos resulting from giant mass movements. In *Sagalassos V. Report on the Survey and Excavation Campaigns of 1996 and 1997*, Waelkens M, Loots L (eds). Acta Archaeologica Lovaniensia Monographiae 11: University Press, Leuven; 783–798.

Waelkens M. 1993. Sagalassos. History and archaeology. In *Sagalassos I. First General Report on the Survey (1986–1989) and Excavations (1990–1991)*, Waelkens M (ed). Acta Archaeologica Lovaniensia Monographiae 5: University Press, Leuven; 37–82.

Waelkens M, Sintubin M, Muchez P, Paulissen E. 2000. Archeological, geomorphological and geological evidence for a major earthquake at Sagalassos (SW Turkey) around the middle of the seventh century AD. In *The Archaeology of Geological Catastrophes*, McGuire WJ, Griffiths DR, Hancock PL, Stewart IS (eds). Special Publication 171: Geological Society Publishing House: Bath; 373–383.

Waelkens M, Paulissen E, Vandeput L, Poblome J, Degeest R, Talloen P, Loots L, Martens F, Uytterhoeven I, Akyel I, Vandenbergh J, Vandamme I, Debruyne T, Erb E, Vandaele B, Roels E, Schiltz M, Licoppe C, Ercan S, Torun E. In press. The 1998, 1999, 2000 and 2001 excavation seasons at Sagalassos. In *Sagalassos VI. Report on the Survey and Excavation Campaigns of 1998, 1999, 2000 and 2001*, Waelkens M, Poblome J (eds). Acta Archaeologica Monographiae Lovaniensia: University Press, Leuven.

Yalcinkaya S. 1983. *Geological map of Isparta—M25-d.1.* Maden Tetkik ve Arama Genel Müdürlügü (General Directorate of Mineral Research and Exploration): Ankara.

